Size distribution of mineral aerosol: using light-scattering models in laser particle sizing

Ben Veihelmann, Martin Konert, and Wim J. van der Zande

The size distribution of semitransparent irregularly shaped mineral dust aerosol samples is determined using a commonly used laser particle-sizing technique. The size distribution is derived from intensity measurements of singly scattered light at various scattering angles close to the forward-scattering direction at a wavelength of 632.8 nm. We analyze the results based on various light-scattering models including diffraction theory, Mie calculations for spheres with various refractive indices, and *T*-matrix calculations for spheroidal particles. We identify systematic errors of the retrieved size distribution when the semitransparent and nonspherical properties of the particles are neglected. Synthetic light-scattering data for a variety of parameterized size distributions of spheres and spheroids are used to investigate the effect of simplifying assumptions made when the diffraction model or Mie theory is applied in the retrieval.

OCIS codes: 120.0120, 120.5820, 010.0010, 010.1100, 010.1110, 290.0290.

1. Introduction

Mineral dust is present in the Earth's atmosphere, hydrosphere, and lithosphere. Many properties of mineral dust depend crucially on the size of the particles. The measurement of the size distribution of mineral dust samples can be difficult due to the irregular shapes of the mineral particles. Here we focus on a commonly used and powerful particle-sizing technique using intensity measurements of singly scattered light, referred to as laser particle sizing in the following. This technique is based on the fact that light scattering close to the forward-scattering direction is sensitive to size but rather insensitive to refractive index and particle shape. The same principle is used for the measurement of the size distribution of an atmospheric aerosol using ground-based sky radiance measurements in the aureole, i.e., in viewing geometries close to the Sun.

Most laser particle-sizing techniques are based either on the so-called diffraction method or on Mie theory.[1,2] The diffraction method is often preferred, since it tends to provide numerically stable results and no assumption regarding the refractive index has to be made. This method assumes that light scattering can be described by Fraunhofer diffraction from round nontransparent disks implicitly neglecting refracted light components. The diffraction model is applicable to particle samples containing nontransparent particles much larger than the wavelength. Mie theory treats spherical particles with arbitrary refractive indices and sizes. Laser particle-sizing techniques using Mie theory or the diffraction method are, hence, based on the assumption that the sample particle is spherical.

Volten *et al*.[3] measured the scattering properties of various mineral dust samples. Most of these samples contain weakly absorbing particles with irregular shapes and a broad size distribution including sizes comparable to the wavelength. The size distributions of these mineral dust samples have been measured using a laser particle sizer (Fritsch Analysette 22-E) with the diffraction method.

In this study, we analyze various light-scattering models in their application to laser particle sizing and determine the effect of the assumptions made on the retrieved size distribution of weakly absorbing nonspherical particles. The size distribution and its

When this research was performed, B. Veihelmann (veilhelmann@gmail.com) was with the Department of Earth Oriented Science, National Institute for Space Research (SRON), Utrecht, The Netherlands. He is now with the Royal Dutch Meteorological Institute, De Bilt, The Netherlands. M. Konert is with the Laboratory for Sediment Analysis, Free University of Amsterdam, The Netherlands. W. J. van der Zande is with the Institute for Molecules and Materials, Radboud University Nijmegen, The Netherlands.

Received 9 January 2006; revised 14 March 2006; accepted 14 March 2006; posted 15 March 2006 (Doc. ID 67122).

0003-6935/06/236022-08$15.00/0

discrete representation used in this study are introduced in Section 2. The concept of laser particle sizing is discussed in Section 3. The optical setup of a typical laser particle sizer is sketched briefly. We develop forward models linking the size distribution of a sample to the measured intensity signal based on various light-scattering models. We discuss inversion schemes used to derive size distributions from intensity measurements. In Section 4, the size distribution of three mineral samples including a feldspar, a quartz, and a red clay sample from real intensity measurements are retrieved using diffraction theory, Mie calculations for spheres with various refractive indices, and T-matrix calculations for spheroidal particles. The discrepancies of the size distributions are discussed and systematic errors and limitations of the methods applied are quantified. The effective radius and the effective variance (for definition see, e.g., Hansen and Travis[4]) of a parameterized lognormal size distribution can be retrieved using a nonlinear least-squares fit routine. Based on a range of synthetic measurements of monomodal parameterized size distributions, systematic errors are determined that are encountered when the diffraction method is applied to strongly absorbing and nonabsorbing spherical particles. In a similar way, we quantify the systematic errors that are encountered when Mie theory is applied to nonspherical particles.

2. Size Distribution

Sizing techniques that are applicable to ensembles of irregular particles are always based on simplifying assumptions concerning the particle shape. One obvious reason is that the exact shape of all particles in a very large ensemble cannot be taken into account explicitly. Furthermore, the laser particle-sizing method discussed here is based on numerical light-scattering models that require a simplified shape description. In the following, we will refer to the size of a particle as the radius r of a sphere with the same volume. We also use the size parameter $x = 2\pi r/\lambda$, where λ is the wavelength of light.

The size distribution of an ensemble of spherical particles can be described by $\nu(R)$ as a function of the log-radius $R = \log_{10}(r)$:

$$\nu(R) = \frac{\mathrm{d}N}{\mathrm{d}\,\log_{10}(r)}. \tag{1}$$

We introduce the normalized and discrete forms of the logarithmic number distribution $\mathbf{n}$ with the elements

$$n_i = \frac{1}{\int_{-\infty}^{+\infty} \nu\,\mathrm{d}R} \int_{R_i}^{R_{i+1}} \nu(R)\mathrm{d}R. \tag{2}$$

The surface distribution $\mathbf{s}$ with

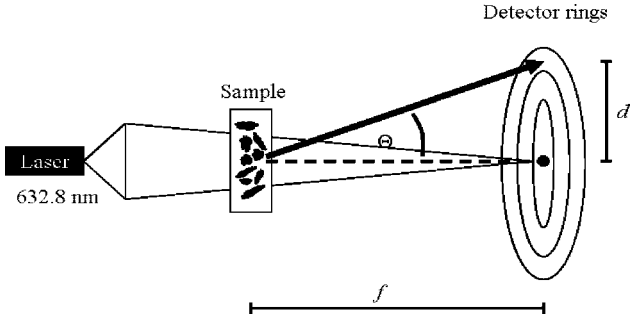

Fig. 1. Optical setup of the laser particle sizer.

$$s_i = \frac{1}{\int_{-\infty}^{+\infty} \pi r^2 \nu\,\mathrm{d}R} \int_{R_i}^{R_{i+1}} \pi r^2 \nu(R)\mathrm{d}R \tag{3}$$

describes the fraction of the ensemble surface that is present in the size range from R_i to R_{i+1}. The surface distribution $\mathbf{s}$ is convenient for laser particle sizing, since the light-scattering cross section of particles with size parameters $x \geq 10$ scales with the particle surface. In natural ensembles of mineral particles, small particles occur much more frequently than larger ones. Natural size distributions of dust aerosol (see, e.g., Dubovik *et al.*[5]) are, thus, very steep and may cover many orders of magnitude when being expressed in terms of a number distribution. This can cause problems in the numerical representation of the number distribution $\nu(R)$. The surface distribution is less steep and is therefore preferred. In the following, the terms surface distribution and size distribution are used synonymously.

3. Forward Model and Inversion Scheme

The optical setup of the laser particle sizer used for the characterization of the mineral samples is sketched in Fig. 1. A widened He–Ne laser with a wavelength of $\lambda = 632.8$ nm is focused on a detector screen. The laser light is directed through a cuvette with a dilute suspension of particles in water. The suspension is continuously renewed from a reservoir, where settling of larger particles is reduced by continuous stirring. The scattered light is focused on a screen and detected by a series of concentric ring-shaped detectors. The radii of the detector rings are chosen to be equidistant on a logarithmic grid such that the logarithm of the detector areas increases with a constant increment. The detectors cover a range of scattering angles from a fraction of a degree to more than 60°. The scattering angle $\Theta = 0°$ denotes forward scattering. The suspension is optically thin, such that multiple scattering is negligible. Since the laser beam is narrow, the radius on the screen d is related to the scattering angle by $\tan(\Theta) = d/f$, where f is the distance between the scatterer and the screen. The measured values of the electromagnetic radiation flux, in the following referred to as intensity, are the observation vector $\mathbf{y}$.

We develop a forward model for the simulation of the measured intensity $\mathbf{y}$ as a function of the size distribution $\mathbf{s}$ of the sample. The intensity y_i measured by the ith detector is calculated by an integration of the phase function $P(\Theta)$ over the solid angle Ω_i of the ith detector:

$$y_i = \sum_j Q_j s_j \int_{\Omega_i} P_j(\Theta)\mathrm{d}\Omega \text{ const.} \tag{4}$$

The contributions of all j sizes to this intensity are weighted with the surface distribution s_i and the scattering efficiency $Q_j = c_j/(\pi r_j^2)$, defined as the ratio of the scattering cross section c_j and the geometrical cross section. The forward model is linear and can be written in matrix notation as

$$\mathbf{y} = \mathbf{K}\mathbf{s} \cdot \text{const.} \tag{5}$$

The constant factor in Eqs. (4) and (5) depends on the total amount of mineral dust measured, the light intensity of the laser, the absolute size of the detectors, or the detector gain, for instance. We may drop this factor, since only the normalized size distributions $\mathbf{s}$ are needed in what follows.

In the following, we highlight differences between various light-scattering models regarding the phase function, the scattering efficiency, and the Jacobian matrix $\mathbf{K}$. In the diffraction model, light scattering is approximated by far-field interference at round nontransparent disks with the radius r. The phase function $P(\Theta)$ is described by the intensity distribution of Fraunhofer interference $I_F(x, \Theta)$ (cf. Born and Wolf[6]):

$$I_F(x, \Theta) \propto x^2 \left\{ \frac{J_1[x \sin(\Theta)]}{x \sin(\Theta)} \right\}^2. \tag{6}$$

The function J_1 denotes the first-order Bessel function of the first kind, whereas x is the size parameter. The diffraction cross section is identical to the geometrical cross section of the disk $c = \pi r^2$. Mie theory treats light scattering by spherical particles. We test models based on Mie scattering for spheres with various refractive indices. We use the refractive indices $1.57 - 0.5i$ for strongly absorbing spheres and $1.57 - 0i$ as well as $1.8 - 0i$ for nonabsorbing spheres. Furthermore, we consider spheres with the refractive indices $1.57 - 0.0005i$, $1.54 - 0i$, and $1.52 - 0.001i$ as estimates for the feldspar, the quartz, and the red clay samples, respectively. These estimates for the refractive indices in a vacuum are based on data from various sources.[7–9] Since the surrounding medium in the particle sizer is water, light-scattering calculations are based on relative values of the real part of the refractive index. T-matrix calculations can be used for spheroidal particles.[10] We consider an ensemble of nonabsorbing prolate and oblate spheroids including aspect ratios ranging from 0.5 to 2. The computing time and the convergence of the T-matrix code pose an upper limit to the applicable size range. This limit decreases with the increasing deviation of the aspect ratio from unity.[11] With the chosen range of aspect ratios, spheroids with volume-equivalent sphere radii of up to 6.5 μm are included in the retrieval. In the following, the size of spheroids will be referred to as the radius of the volume-equivalent sphere. This light-scattering model will be referred to as the spheroidal model.

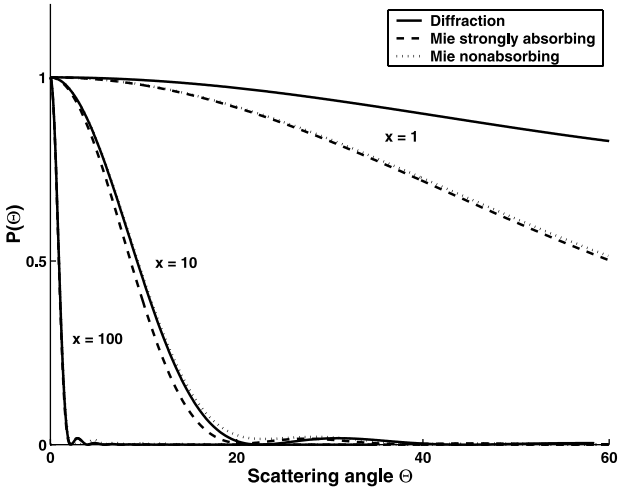

Fig. 2. Phase function $P(\Theta)$ for diffraction (solid curves) and Mie scattering by strongly absorbing (dashed curves) and nonabsorbing spheres (dotted curves). The intensity is normalized to 1 at $\Theta = 0°$. The sizes of the spheres are given in terms of the size parameter $x = 2\pi r/\lambda$.

In Fig. 2, the phase functions based on diffraction (solid curves), Mie scattering by strongly absorbing (dashed curves) and nonabsorbing spheres (dotted curves) are shown for the size parameters 1, 10, and 100. For demonstrative purposes, the phase functions are normalized to 1 at $\Theta = 0°$. The width of the intensity peak centered at $\Theta = 0°$ is inversely proportional to the particle size. It is possible to distinguish particles with different sizes in light-scattering experiments mainly due to this property. We note differences between the phase functions derived from diffraction theory and from Mie theory, especially for small particles (see the graph for $x = 1$).

The scattering efficiency Q of strongly absorbing spheres (solid circles), nonabsorbing spheres (empty circles), and nonabsorbing spheroids (dots) are shown as a function of the particle size (Fig. 3.) The scattering efficiency that is attributed to the diffraction model (crosses) takes the constant value unity. In contrast to two-dimensional disks, the scattering efficiency of spherical and nonspherical particles is clearly size dependent. The scattering efficiency has very small values ($Q \ll 1$) at $x = 1$, increases to a maximum at $x \approx 10$, and after some oscillations approaches a constant value. For nonabsorbing spheres and spheroids, the maximum scattering efficiency has a value of about 3.6 and the oscillations are pronounced. A maximum of this amplitude is found as well in the scattering efficiency of weakly absorbing particles with other shapes with no symmetry such as Gaussian

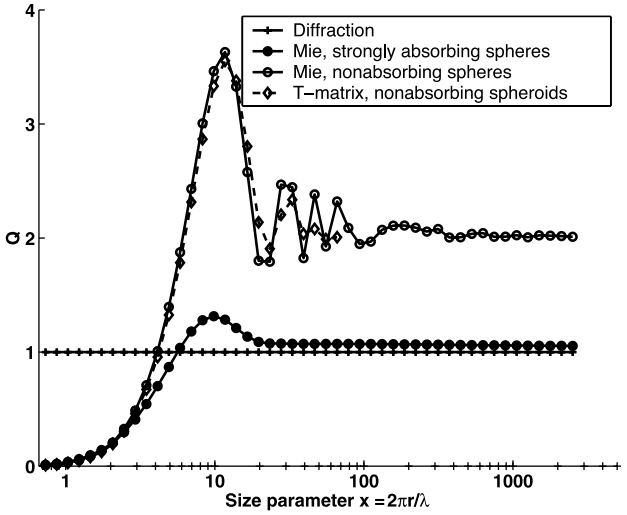

Fig. 3. Scattering efficiency Q for diffraction (crosses), from Mie calculations for strongly absorbing spheres (solid circles), from nonabsorbing spheres (open circles), and from T-matrix calculations for nonabsorbing spheroids (open diamonds).

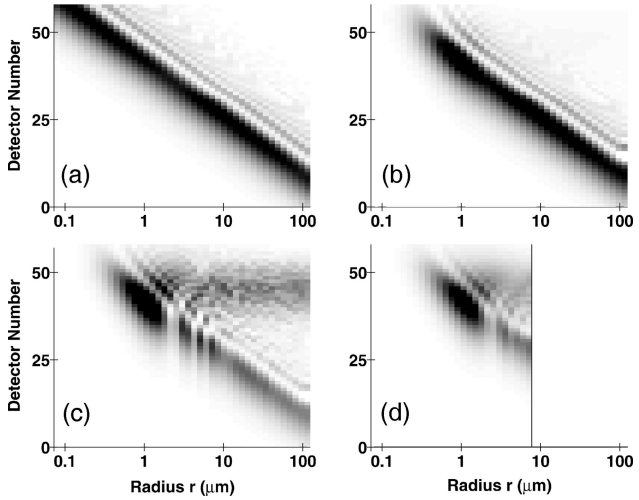

Fig. 4. Representation of the Jacobian matrix of the linearized forward model based on (a) diffraction theory, Mie theory for (b) strongly absorbing spheres and (c) nonabsorbing spheres, and (d) T-matrix calculations for a mixture of nonabsorbing oblate and prolate spheroids. High values of the matrix elements K_{ij} are depicted as dark gray; low values are depicted as light gray levels. Further explanations are given in the text.

random spheres.[12] An asymptotic value of about 2 is reached for size parameters of $x \geq 200$ in the geometric optics domain. For strongly absorbing particles, the maximum scattering efficiency is lower ($Q \approx 1.4$) and a constant value of $Q \approx 1$ is reached for size parameters of $x \geq 2$. Measurements of the extinction efficiency of quartz and diamond dust samples as well as other powdery substances indicate that the scattering efficiency of natural irregular particles exhibit the characteristic first maximum shown by the spherical model and the spheroidal model (Bohren and Huffman,[13] Section 11.7.3 and references therein).

In Fig. 4, we show the Jacobian matrices $\mathbf{K}$ of the diffraction model [Fig. 4(a)], and the models for strongly absorbing spheres [Fig. 4(b)], nonabsorbing spheres [Fig. 4(c)], and nonabsorbing spheroids [Fig. 4(d)]. The element (0, 0) of the matrices is depicted at the lower left corner of each graph. This element $K_{00} = \partial y_0/\partial s_0$ represents the sensitivity of the innermost detector ring with respect to the surface distribution at the smallest particle size. Matrix elements with a large amplitude are depicted in dark gray. Note that the measured intensity vectors, i.e., the column vectors $K_{i1}, K_{i2}, \ldots$ have low values at the inner detector rings even though the phase function generally has the largest values close to $\Theta = 0°$. This is due to the geometry of the detector rings in which the detector areas increase logarithmically with increasing detector number i.

The Jacobian matrix of the diffraction model $\mathbf{K}_a$ has a simple structure. We note that the inner detectors are sensitive mainly to large particles, whereas the outer detectors are sensitive mainly to small particles. This is related to the fact that the particle sizes of the size distribution $\mathbf{n}$ as well as the detector areas are chosen to be equidistant on a logarithmic grid. Due to the simple near-diagonal structure of $\mathbf{K}_a$, the diffraction model provides comparatively stable results and is therefore preferably used in laser particle-sizing techniques. The Jacobian matrix of the model for strongly absorbing spheres $\mathbf{K}_b$ is similar to the Jacobian matrix of the diffraction model $\mathbf{K}_a$ for particle sizes with $x > 10$. For smaller particle sizes, the amplitudes of the column vectors of $\mathbf{K}_b$ decrease with decreasing particle size, which is not the case for $\mathbf{K}_a$. This difference is due to the discrepancy in the scattering efficiency of the models shown in Fig. 3. The pronounced size dependence of the scattering efficiency of the model for nonabsorbing spheres is reflected in the amplitudes of the column vectors of $\mathbf{K}_c$. As compared to $\mathbf{K}_b$, the elements of $\mathbf{K}_c$ (nonabsorbing spheres) that are related to detectors 40 to 50 have large values. This is related to the more pronounced sideward scattering of nonabsorbing spheres. The spheroidal model is limited in particle size due to the convergence limit of the T-matrix code. In the size range considered (from $x = 1$ to 65), the Jacobian matrices for nonabsorbing spheroids $\mathbf{K}_d$ and nonabsorbing spheres $\mathbf{K}_c$ are similar. Note the similarity in the resonant structures that are revealed by the wavy nature of the graphs.

The forward model $\mathbf{y} = \mathbf{Ks}$, derived in Section 2, is linear. The retrieval of the size distribution is equivalent to finding an inverse matrix $\mathbf{D}$ to the matrix $\mathbf{K}$ that relates a size distribution to a given measurement

$$\mathbf{s} = \mathbf{Dy}. \tag{7}$$

The number of sizes (n) is usually chosen to be smaller than the number of detectors (m). In this case, the matrix $\mathbf{K}$ is not square, and the simple inverse matrix $\mathbf{K}^{-1}$ is not defined. A least-squares solution can be derived using the maximum likelihood method. This approach is based on the assump-

tion that errors are Gaussian distributed, which can be supported by minimum entropy considerations (e.g., Rodgers[14]). To obtain a stable and physically meaningful result, we include *a priori* information about the solution. This can be done by applying the Phillips–Tikhonov regularization[15,16] in the form

$$\mathbf{D} = \left[\mathbf{K}^T\mathbf{S_y}^{-1}\mathbf{K} + \gamma_0\mathbf{L_0}^T\mathbf{L_0} + \gamma_1\mathbf{L_1}^T\mathbf{L_1}\right]^{-1}\mathbf{K}^T\mathbf{S_y}^{-1}. \quad (8)$$

The matrix $\mathbf{S_y}$ is the error covariance matrix of the measurement. The diagonal elements are the variances σ_{yi}^2 of the measurements and are assumed to be 2% of the largest intensity measured. The off-diagonal elements are zero since the detector errors are uncorrelated. $\mathbf{L_0}$ is the unity matrix and $\mathbf{L_1}$ is the discrete difference matrix

$$\mathbf{L_1} = \begin{pmatrix} 1 & -1 & 0 & \dots & 0 \\ 0 & 1 & -1 & & \vdots \\ \vdots & & \ddots & \ddots & 0 \\ 0 & \dots & 0 & 1 & -1 \end{pmatrix} \quad (9)$$

with the dimensions $(n - 1) \times n$. The second and third terms on the right-hand side are responsible for a smoothing of the solution. The Lagrange multipliers γ_0 and γ_1 control the weight of the smoothing conditions and are chosen as follows. The ratio of γ_0 and γ_1 is of the same order of magnitude as recommended by Dubovik and King.[17] For an optimal choice of the magnitudes, we consider the number of degrees of freedom N_f of the solution that are determined by the measurement. The number of degrees of freedom is determined based on the averaging kernel $\mathbf{A} = \mathbf{DK}$ being the product of the Jacobian matrix $\mathbf{K}$ of the forward model with the generalized inverse matrix $\mathbf{D}$.[14] This matrix represents the sensitivity of the retrieved size distribution with respect to the true (unknown) size distribution.[18] The trace of the matrix $\mathbf{A}$ gives the number of degrees of freedom of the solution N_f, which are determined by the measurement (rather than by the constraints applied). We use one set of values for the Lagrange multipliers for all retrievals such that the solutions are stable and smooth. The solutions based on Mie and diffraction theory have 41 bins with about 7 degrees of freedom. The solutions based upon using *T*-matrix calculations have 27 bins with about 4 degrees of freedom.

4. Results

In this section, we discuss size distributions obtained using the diffraction model, Mie theory, and the spheroidal model. First, we compare retrieved size distributions using real light-scattering measurements of three mineral samples. Second, we compare parameterized size distributions retrieved from a variety of simulated measurements with a range of effective radii and effective variances.

In Fig. 5, we show the size distributions of the feldspar, the quartz, and the red clay samples that are retrieved from the intensity measurements using

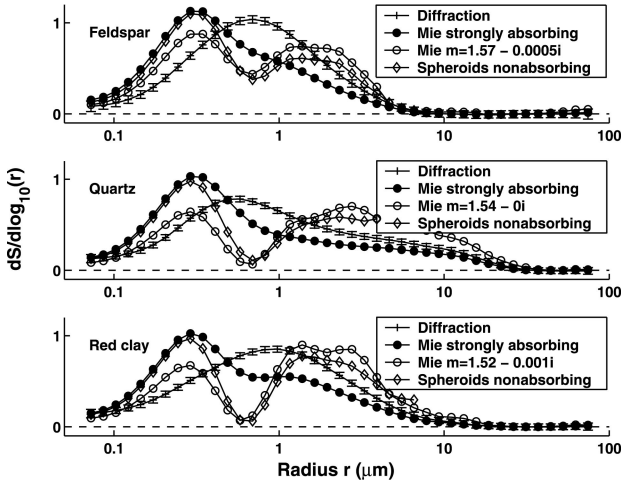

Fig. 5. Surface distributions for the feldspar, the quartz, and the red clay samples retrieved using diffraction theory (error bars); Mie scattering by strongly absorbing spheres (black dots); by weakly absorbing spheres (open circles) assuming refractive indices of $1.57 - 0.0005i$ (feldspar), $1.54 - 0i$ (quartz), and $1.52 - 0.001i$ (red clay); and *T*-matrix calculations for nonabsorbing spheroids (open diamonds).

diffraction theory (with error bars), Mie calculations for strongly absorbing spheres (black dots), Mie calculations for weakly absorbing spheres (open circles), and *T*-matrix calculations for nonabsorbing spheroids (open diamonds). The results of the diffraction method are shown with error bars representing the standard deviation of the error due to instrument noise σ_s. The variances σ_s^2 are the diagonal elements of the error covariance matrix $\mathbf{S_s}$:

$$\mathbf{S_s} = \left(\mathbf{K}^T\mathbf{S_y}^{-1}\mathbf{K} + \gamma_0\mathbf{L_0}^T\mathbf{L_0} + \gamma_1\mathbf{L_1}^T\mathbf{L_1}\right)^{-1}. \quad (10)$$

The errors of the size distributions determined using Mie and *T*-matrix calculations (not shown) have an amplitude similar to the errors of the results from the diffraction theory. The results using Mie calculations for weakly absorbing spheres are based on the refractive indices $1.57 - 0.0005i$ (feldspar), $1.54 - 0i$ (quartz), and $1.52 - 0.001i$ (red clay). Retrievals using Mie calculations for spheres with various refractive indices show that the retrieved size distributions are insensitive with respect to variations of the refractive index in the range from 1.52 to 1.8 (real part) and from 0 to 0.001 (imaginary part).

The results for spherical and spheroidal models deviate significantly from the results obtained using diffraction theory. The size distribution based on Mie scattering by weakly absorbing spheres has a pronounced minimum at the particle radii between 0.5 and 1 μm. This minimum is also present in the size distribution based on Mie scattering by strongly absorbing spheres but is less pronounced. The size distributions based on the diffraction model do not exhibit this minimum at all. This discrepancy is observed for all three samples and can be explained by two effects: First, at the particle sizes where a light-

scattering model underestimates the scattering efficiency, it overestimates the size distribution. This is the case for the diffraction model and to a lesser degree for Mie theory for strongly absorbing spheres, in the size range from $r = 0.5$ to 2 μm ($x = 5$ to 20) if weakly absorbing spheres or spheroids are present (see Fig. 3). Second, the enhanced sideward scattering of weakly absorbing spheres or spheroids with radii larger than 1 μm causes a light-scattering signal with a secondary maximum between detectors 40 and 50 [Fig 4(c)]. This light-scattering signal is assigned to particles in the size range between 0.5 and 1 μm if the diffraction model of Mie theory for strongly absorbing spheres is applied.

To show that this discrepancy is a systematic feature due to the different nature of the models used, we perform retrievals from synthetic measurements, which are forward simulated based on Mie theory using a lognormal size distribution of spheres with a refractive index of $1.52 - 0.001i$ with $r_{\text{eff}} = 3$ μm and $v_{\text{eff}} = 3$. Indeed, the retrieval scheme based on diffraction overestimates the size distribution at radii between 0.5 and 1 μm as compared to Mie theory. As a consistency check, we compare the initial size distribution as well with a retrieval based on Mie calculations for spheres with the same refractive index. The initial size distribution is well reproduced for spheres with radii of $r \geq 0.3$ μm and overestimated for smaller radii. The retrieved values for $r < 0.3$ μm are not meaningful, as will be discussed in detail in the following.

The retrieved size distributions are partly determined by the smoothness constraint, as can be shown using the averaging kernel matrix **A**. The near-diagonal elements of the averaging kernel of the diffraction model have finite positive values, whereas the other elements vanish [Fig. 4(a)]. Hence the results of the diffraction model are representative for the true size distribution on the full size range considered, provided that the light scattering is accurately modeled by the diffraction model. The shape of the averaging kernels shown in Figs. 4(b)–4(d) indicates that the spherical and the spheroidal models provide reliable results for particle radii larger than approximately 0.3 μm. The insensitivity below 0.3 μm is related to the fact that the phase function of arbitrary particles approaches the phase function $P_{\text{Ray}}(\Theta) \propto \cos^2(\Theta)$ of Rayleigh scattering with decreasing particle size. The values of the size distributions for $r < 0.3$ μm determined using Mie theory or the spheroidal model are not meaningful, and the shape of the size distribution is dominated by the smoothness constraints.

The size distributions using Mie theory or the spheroidal model increase with decreasing radius in the size range of $0.3\ \mu\text{m} < r < 0.6\ \mu\text{m}$ indicating the presence of a small particle mode. According to the averaging kernel, the values of the size distribution in this size range are meaningful. Retrievals for a mineral dust sample where the small particle fraction ($r < 0.5$ μm) has been removed do not show this small particle mode. Therefore we regard the presence of a small particle mode in the size distribution shown here to be real. We note that the shape of the resulting size distributions agrees well with the shape of size distributions retrieved from atmospheric Sun and sky radiometer measurements at desert sites.[5,19] These retrievals are based on light scattering and absorption measurement at various wavelengths and geometries.

Table 1. Effective Radius r_{eff} (μm) and Effective Variance v_{eff} of the Size Distributions Based on the Diffraction Model and the Spherical Model[a]

	Diffraction		Mie		Mie Truncation	
	r_{eff}	v_{eff}	r_{eff}	v_{eff}	r_{eff}	v_{eff}
Feldspar $m = 1.57 - 0.0005i$	1.0	0.9	0.5	2.5	1.4	0.6
Quartz $m = 1.54 - 0i$	2.3	2.4	1.6	4.1	4.4	1.0
Red clay $m = 1.52 - 0.001i$	1.5	2.3	0.9	3.4	2.4	0.8

[a]The right column refers to a size distribution that is truncated at the size parameter $x = 3$.

The effective radii and the effective variances of the retrieved size distributions for the three mineral samples are listed in Table 1. We compare the results based on the diffraction model with the results based on the spherical model using estimates for the refractive indices of the mineral samples. For the spherical model, we include the size distribution shown in Fig. 5 as well as a size distribution that is truncated at the radius 0.3 μm. With the latter two size distributions, we include two extreme cases that are consistent with the measurement. The range of effective radii and effective variances defined by these two extreme cases includes the effective radius and the effective variance of the size distributions derived using the diffraction model.

In this section, synthetic light-scattering data for a variety of size distributions of spheres or spheroids are considered. Measurements of the laser particle sizer are simulated based on a monomodal lognormal size distribution with the effective radius r_{eff} and the effective variance v_{eff} as parameters. The simulations for spheres cover a range of effective radii from 0.5 to 5 μm and a range of effective variances from 0.5 to 6. Simulations for spheroids are made for effective radii ranging from 0.5 to 2 μm and for effective variances ranging from 0.5 to 1.5. The parameters r_{eff} and v_{eff} are retrieved from the synthetic measurements using the diffraction model or Mie theory. The retrieval is performed using an advanced nonlinear fit routine that is based on a large-scale trust region method.[20]

For strongly absorbing spheres in the size range considered in this study, the diffraction model provides realistic size parameters only if the effective variance is lower than unity. Otherwise, the retrieval is biased by small particles with a light-scattering behavior, which significantly deviates from diffraction. In this case, the effective radius is underestimated for $r_{\text{eff}} >$

3 μm and overestimated for $r_{eff} < 2$ μm. The effective variance is underestimated, while the error increases with the increasing value of v_{eff}.

If nonabsorbing spheres are present, the diffraction model underestimates the effective radius for initial values of $r_{eff} > 2$ μm. The effective variance is underestimated except for the regime with $r_{eff} > 3$ μm and $v_{eff} < 1.5$. The errors in the retrieved effective radius and the retrieved effective variance are nearly proportional to their true values, respectively.

If nonabsorbing spheroidal particles are present, the model using nonabsorbing spheres provides good estimates for the effective radius and the effective variance except for two regimes. These regimes include narrow size distributions with particle radii in the range from 1 to 1.5 μm and size distributions with r_{eff} close to 0.5 μm and $v_{eff} > 1$. In the size range with radii from 1 to 1.5 μm, Mie scattering has pronounced resonance features in the scattering efficiency (Fig. 3) as well as in the phase function, which are less pronounced for scattering by spheroidal particles. This causes errors of the retrieved parameters for narrow size distributions. For broader size distributions, these discrepancies average out.

5. Conclusions

The size distributions of mineral aerosol samples including feldspar, quartz, and red clay have been retrieved from light-scattering measurements of a laser particle sizer. For the retrieval, we applied various light-scattering models including diffraction theory, Mie theory for spherical particles with various refractive indices, and *T*-matrix calculations for nonabsorbing spheroidal particles.

The models based on Mie and *T*-matrix calculations for spheres and spheroids provide stable results for volume-equivalent sphere radii of $r \geq 0.3$ μm. For smaller radii, the size distribution is governed by the smoothness constraints applied in the retrieval. The limit at $r \approx 0.3$ μm is what can be expected in view of the wavelength of the laser used (0.63 μm). For larger radii, the size distributions based on Mie theory are insensitive with respect to variations of the refractive index in the range from 1.52 to 1.8 (real part) and from 0 to −0.001 (imaginary part). This covers the range of uncertainty of the imaginary part of the refractive index of the mineral samples measured, which is estimated to be from 1.5 to 1.6 (real part) and 0 to −0.001 (imaginary part). The size distribution of nonabsorbing particles appears to be rather insensitive with respect to the particle shape: for radii of $r \leq 6.5$ μm, the results of retrievals using spheres or spheroids are similar. This indicates that the size distributions based on Mie calculations for weakly absorbing spheres are representative for the true size distributions of the samples measured, provided that the light scattering is sufficiently well described by light-scattering simulations using homogeneous model particles.

The retrieval based on diffraction theory systematically overestimates the size distribution at radii between $r = 0.5$ μm and $r = 1$ μm as compared to retrievals based on models for weakly absorbing spheres or spheroids. This has been shown for a variety of refractive indices including values from 1.52 to 1.8 for the real part of the refractive index. This systematic discrepancy is caused by the enhanced sideward scattering and the prominent maximum of the scattering efficiency close to $r = 1$ μm, which is neglected when diffraction theory is used. Light-scattering simulations for Gaussian random shapes show that a similar maximum in the scattering efficiency is found as well for weakly absorbing homogeneous particles with no symmetry.[12] Experimental evidence for the presence of such a maximum in the extinction efficiency of irregular particles has been given for quartz and diamond dust samples as well as for other powdery substances (Bohren and Huffman,[3] Section 11.7.3 and references therein). This suggests that the diffraction model introduces a systematic error in the size distribution of natural irregular dust containing particles with sizes comparable to the wavelength, especially if the absorption is low.

The size distributions of our three samples derived using light-scattering models for weakly absorbing homogeneous spheres or spheroids exhibit a pronounced bimodality. Bimodal size distributions have also been observed for atmospheric mineral aerosols using Sun and sky radiometer measurements at desert sites using Mie theory or a spheroidal model.[5,19] These data are independent of our results in the sense that they are derived from atmospheric light scattering and extinction measurements at various wavelengths. A bimodal size distribution has also been derived from extinction measurement of dusty air masses over Eastern Europe.[21] The question is whether this bimodality reflects the truth or whether it is a systematic error caused by the assumption that the particles are homogeneous. This cannot be decided conclusively without an efficient light-scattering model that can handle irregular-shaped particles with internal inhomogeneities or independent size measurements. At this point, we can conclude that the size distributions derived from the laser particle sizer using Mie theory are a useful estimate for the mineral samples considered.

Simulations using simple model shapes have been exploited to evaluate light-scattering models in the context of laser particle sizing. Based on the observed trends, one may extrapolate the results to truly irregular particles with internal inhomogeneities, as they are present in natural mineral dust. An efficient light-scattering model that can handle truly irregular particles including internal inhomogeneities is still lacking as a reliable reference. Therefore we would like to encourage nephelometer and extinction measurements of size-resolved irregular particle samples.

References

1. M. Kocifaj and M. Držík, "Retrieveing the size distribution of microparticles by scanning the diffraction halo with a mobile ring gap detector," J. Aerosol Sci. **28,** 797–804 (1996).
2. R. Santer and M. Herman, "Particle size distributions from

forward scattered light using the Chahine inversion scheme," Appl. Opt. **22,** 2294–2301 (1983).
3. H. Volten, O. Muñoz, E. Rol, J. F. de Haan, W. Vassen, J. W. Hovenier, K. Muinonen, and T. Nousiainen, "Scattering matrices of mineral particles at 441.6 nm and 632.8 nm," J. Geophys. Res. **106,** 17375–17401 (2001).
4. J. E. Hansen and L. D. Travis, "Light scattering in planetary atmospheres," Space Sci. Rev. **16,** 527–610 (1974).
5. O. Dubovik, B. N. Holben, T. F. Eck, A. Smirnov, Y. J. Kaufman, M. D. King, D. Tanré, and I. Slutsker, "Variability of absorption and optical properties of key aerosol types observed in worldwide locations," J. Atmos. Sci. **59,** 590–608 (2002).
6. M. Born and E. Wolf, *Principles of Optics,* 7th ed. (Cambridge U. Press, 1999).
7. D. R Huffman, "The interaction of light with a small-particle system," Adv. Phys. **26,** 129–130 (1977).
8. I. N. Sokolik and O. B. Toon, "Incorporation of mineralogical composition into models of the radiative properties of mineral aerosol from UV to IR wavelengths," J. Geophys. Res. **104,** 9423–9444 (1999).
9. C. Klein, *Manual of Mineral Science,* 22nd ed. (Wiley, 2002).
10. M. I. Mishchenko J. W. Hovenier, and L. D. Travis, "*T*-matrix method and its applications," in *Light Scattering by Nonspherical Particles,* M. I. Mishchenko, J. W. Hovenier, and L. D. Travis, eds. (Academic, 2000), pp. 147–172.
11. M. I. Mishchenko and L. D. Travis, "Capabilities and limitations of a current FORTRAN implementation of the *T*-matrix method for randomly oriented, rotationally symmetric scatterers," J. Quant. Spectrosc. Radiat. Transfer **60,** 309–324 (1998).
12. B. Veihelmann, T. Nousiainen, M. Kahnert, and W. J. van der Zande, "Light scattering by small feldspar particles simulated using the discrete dipole approximation for Gaussian random spheres," J. Quant. Spectrosc. Radiat. Transfer **100,** 393–405 (2006).
13. C. F. Bohren and D. R. Huffman, *Absorption and Scattering of Light by Small Particles* (Wiley, 1983).
14. C. D. Rodgers, *Inverse Methods for Atmospheric Sounding: Theory and Practice* (World Scientific, 2000).
15. D. L. Phillips, "A technique for the numerical solution of certain integral equations of the first kind," J. Assoc. Comput. Math. **9,** 84–97 (1962).
16. A. N. Tikhonov, "On the solution of incorrectly stated problems and a method of regularization," Dokl. Acad. Nauk SSSR **151,** 501–504 (1963).
17. O. Dubovik and M. D. King, "A flexible inversion algorithm for retrieval of aerosol optical properties from Sun and sky radiance measurements," J. Geophys. Res. **105,** 20673–20696 (2000).
18. C. D. Rodgers, "Characterization and error analysis of profiles retrieved from remote sounding measurements," J. Geophys. Res. **95,** 5587–5595 (1990).
19. D. Tanré, Y. J. Kaufman, B. N. Holben, B. Chatenet, A. Karnieli, F. Lavenu, L. Blarel, O. Dubovik, L. A. Remer, and A. Smirnov, "Climatology of dust aerosol size distribution and optical properties derived from remotely sensed data on the solar spectrum," J. Geophys. Res. **106,** 18205–18217 (2001).
20. T. F. Coleman and Y. Li, "An interior, trust region approach for non-linear minimization subject to bounds," SIAM J. Optim. **27,** 960–967 (1970).
21. M. Kocifaj and H. Horvath, "Inversion of extinction data for irregularly shaped particles," Atmos. Environ. **39,** 1481–1495 (2005).